Chapter 3
Performance Evaluation of Vibration-Based Piezoelectric Energy Scavengers

Yi-Chung Shu

Abstract This chapter summarizes several recent activities for fundamental understanding of piezoelectric vibration-based energy harvesting. The developed framework is able to predict the electrical behavior of piezoelectric power harvesting systems using either the standard or the synchronized switch harvesting on inductor (SSHI) electronic interface. In addition, some opportunities for new devices and improvements in existing ones are also pointed here.

3.1 Introduction

The development of wireless sensor and communication node networks has received great interests in research communities over the past few years (Rabaey et al. 2000). Applications envisioned from these node networks include building the health monitoring for civil infrastructures, environmental control systems, hazardous materials detection, smart homes, and homeland security applications. However, as the networks increase in the number and the devices decrease in the size, the proliferation of these autonomous microsensors raises the problem of effective power supply. As a result, the foremost challenge for such dense networks to achieve their full potential is to manage power consumption for a large number of nodes.

Unlike cellphones and laptops, whose users can periodically recharge, embedded devices must operate in their initial batteries. However, batteries cannot only increase the size and weight of microsensors but also suffer from the limitations of a brief service life. For example, at an average power consumption of 100 μW (an order of magnitude smaller than any existing node), a sensor node would last only 1 yr if a 1 cm^3 of lithium battery (at the maximum energy density of 800 W hr per L) was used to supply power (Kansal & Srivastava 2005, Roundy et al. 2005). A lifetime of approximately 1 yr is obviously not practical for many applications. In addition, the need for constant battery replacement can be very tedious and expensive task. In many other cases, these operations may be prohibited by the

Y.C. Shu (✉)
Institute of Applied Mechanics, National Taiwan University, Taipei 106, Taiwan, ROC
email: yichung@spring.iam.ntu.edu.tw

S. Priya, D.J. Inman (eds.), *Energy Harvesting Technologies*,
DOI 10.1007/978-0-387-76464-1_3 © Springer Science+Business Media, LLC 2009

infrastructure. Therefore, energy supply using batteries is currently a major bottleneck for system lifetime, and harvesting energy from the deployment environment can help to relieve it.

Simultaneous advances in low-power electronic design and fabrication have reduced power requirements for individual nodes, and therefore, allow the feasibility of self-powering these autonomous electronic devices. This stems from the fact that power consumption in integrated circuits (IC) will continue to decrease as IC processing moves towards smaller feature sizes (Chandrakasan et al. 1998, Yoon et al. 2005). This opens the possibility for completely self-powered sensor nodes, and the notion of a small smart material generator-producing enough power is not far fetched. However, these smart material generators need to be optimally designed, which is the central topic discussed in this chapter. The goal here is to develop a smart architecture which utilizes the environmental resources available for generating electrical power. These resources include solar power, thermal gradients, acoustic, and mechanical vibration (Roundy et al. 2004a, Sebald et al. 2008, Whalen et al. 2003). Among these energy scavenging sources, we are particularly interested in mechanical vibration since it is a potential power source that is abundant enough to be of use, is easily accessible through microelectromechanical systems (MEMS) technology for conversion to electrical energy, and is ubiquitous in applications from small household appliances to large infrastructures (Roundy et al. 2004b, Sodano et al. 2004).

Vibration energy can be converted into electrical energy through piezoelectric, electromagnetic, and capacitive transducers (Beeby et al. 2007, Cheng et al. 2007, Lee et al. 2004, Nakano et al. 2007, Poulin et al. 2004, Roundy et al. 2003, Stephen 2006a,b, Williams & Yates 1996, Zhao & Lord 2006). Among them, piezoelectric vibration-to-electricity converters have received much attention, as they have high-electromechanical coupling and no external voltage source requirement, and they are particularly attractive for use in MEMS (Choi et al. 2006, Fang et al. 2006, Horowitz et al. 2006, Jeon et al. 2005, Lu et al. 2004). As a result, the use of piezoelectric materials for scavenging

energy from ambient vibration sources has recently seen a dramatic rise for power harvesting (duToit et al. 2005, Elvin et al. 2006, Guyomar et al. 2005, Hu et al 2007a, Kim et al. 2005a, Liao et al. 2001, Ng & Liao 2005, Ottman et al. 2002, Richards et al. 2004, Richter et al. 2006, Roundy & Wright 2004, Shu & Lien 2006a, Sodano et al. 2006). The optimum design and setup of an energy harvesting system using piezoelectric generators depends on the kind of the surrounding kinetic energy to be exploited (amplitude and frequency) as well as on the electrical application to be powered. Thus, it is necessary to use the model-based design methods instead of using try-and-error schemes. To realize such design models, a good understanding of the piezoelectric energy harvesting system is inevitable.

To be precise, an energy conversion device considered here includes a vibrating piezoelectric structure together with an energy storage system, as shown in Fig. 3.1. The piezoelectric generator is modeled as a mass+spring+damper+ piezostructure and is connected to a storage circuit system. An AC–DC rectifier followed by a filtering capacitance C_e is added to smooth the DC voltage. A controller placed between the rectifier output and the battery is included to regulate the

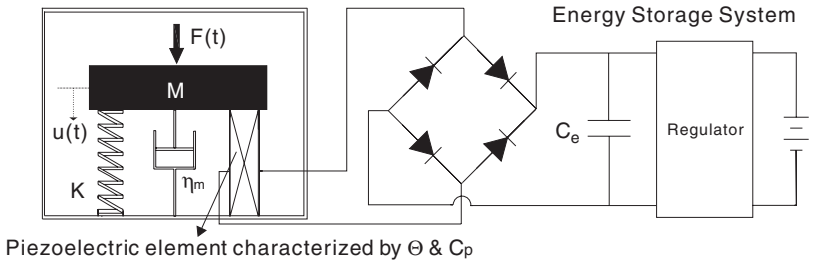

Fig. 3.1 An equivalent model for a piezoelectric vibration energy harvesting system

output voltage. From Fig. 3.1, it is clear to see that the left-hand side is related to the design of piezoelectric power generators and the right-hand side is associated with the design of power electronics. Indeed, current piezoelectric-harvesting research falls mainly into two key areas: developing optimal energy harvesting structures and highly efficient electrical circuits to store the generated charges (Johnson & Clark 2005). The former includes the works by duToit et al. (2005), Lu et al. (2004), Richards et al. (2004), Roundy & Wright (2004), Sodano et al. (2004), and the latter contains the works by Guan & Liao (2007), Lefeuvre et al. (2005b), Ngo et al. (2006), Ottman et al. (2002), Ottman et al. (2003). However, the linkage between these two has not been exploited in detail until recently by Ottman et al. (2002) and Guyomar et al. (2005). They have provided different estimations of AC–DC power output. The former has assumed that the vibration amplitude is not affected by the load resistance, while the latter has hypothesized that the periodic external excitation and the speed of mass are in-phase. In contrast with the estimates based on these two approaches, Shu & Lien (2006a) have provided an analysis of AC–DC power output for a rectified piezoelectric harvester. They have proposed a new method to determine AC–DC power flow without the uncoupled and in-phase assumptions and concluded that their estimation is more accurate than the other two. In addition, Shu & Lien (2006b) have also shown that the conversion efficiency and optimization criteria vary according to the relative strength of the electromechanical coupling and mechanical damping ratio. These results are crucial for the choice of the optimal power converter.

Interest in the application of piezoelectric vibration-based energy scavengers for converting mechanical energy to electrical energy has increased significantly in the very recent years. An overview of research in this field has recently been provided by Sodano et al. (2004) and Anton & Sodano (2007) for review articles as well as by Roundy et al. (2004b) for an advanced book. The following summarizes recent activities in energy harvesting using piezoelectric materials.

3.1.1 Piezoelectric Bulk Power Generators

An early work at MIT Media Lab has investigated the feasibility of harnessing energy parasitically from various human activities (Starner 1996). It was later confirmed that energy generated by walking can be collected using piezoelectric

ceramics (Shenck & Paradiso 2001). Since then, piezoelectric elements used for power harvesting in various forms of structures have been proposed to serve specific purposes. Subsequent studies for generating electricity from walking with loads were discussed by Rome et al. (2005) and Kuo (2005). Granstrom et al. (2007) investigated energy harvesting from a backpack instrumented with piezoelectric shoulder straps. (Elvin et al. 2001, 2003) and Ng & Liao (2005) used the piezoelectric element simultaneously as a power generator and a sensor. They evaluated the performance of the piezoelectric sensor to power wireless transmission and validated the feasibility of the self-powered sensor system. Elvin et al. (2006) further provided the evidence of ability of the harvesting electrical energy generated from the vibration of typical civil structures such as bridges and buildings. Roundy & Wright (2004) analyzed and developed a piezoelectric generator based on a two-layer bending element and used it as a basis for generator design optimization. Renaud et al. (2007) investigated the performances of a piezoelectric bender for impact or shock energy harvesting. Similar ideas based on cantilever-based devices using piezoelectric materials to scavenge vibration energy included the works by Ajitsaria1 et al. (2007), Cornwell et al. (2005), Hu et al. (2007), Jiang et al. (2005), Mateu & Moll (2005), Mossi et al. (2005), and Yoon et al. (2005).

Instead of 1D design, Kim et al. (2005a,b), and Ericka et al. (2005) have modeled and designed piezoelectric plates (membranes) to harvest energy from pulsing pressure sources. Yang et al. (2007) analyzed a rectangular plate piezoelectric generator. Guigon et al. (2008a) and Guigon et al. (2008b) studied the feasibility of scavenging vibration energy from a piezoelectric plate impacted by water drop. Other harvesting schemes included the use of long strips of piezoelectric polymers (Energy Harvesting Eel) in ocean or river-water flows (Allen & Smits 2001, Taylor et al. 2001), the use of ionic polymer metal composites (IPMCs) as generating materials (Brufau-Penella et al. 2008), the use of piezoelectric "cymbal" transducers operated in the $\{3–3\}$ mode (Kim et al. 2004, 2005), the use of drum transducer (Wang et al. 2007), and the use of a piezoelectric windmill for generating electric power from wind energy (Priya 2005, Priya et al. 2005).

3.1.2 Piezoelectric Micro Power Generators

Jeon et al. (2005) and Choi et al. (2006) at MIT have successfully developed the first MEMS-based microscale power generator using a $\{3–3\}$ mode of PZT transducer. A 170 μm $\times$ 260 μm PZT beam has been fabricated and a maximum DC voltage of 3 V across the load 10.1 MΩ has been observed. In addition, the energy density of the power generator has been estimated at around 0.74 mW h/cm^2, which compares favorably to the use of lithium–ion batteries. Fang et al. (2006) subsequently fabricated another MEMS-based microscale power generator utilizing a PZT thick film as the transducer to harvest ambient vibration energy. The dimension of their beam is around 2000 μm $\times$ 500 μm (length $\times$ width) with 500 μm $\times$ 500 μm (length $\times$ height) metal mass. Different from the previous group, a $\{3–1\}$ piezo-mode is operated in their design. The natural frequency is amazingly reduced to only 609 Hz

which is two orders of magnitude smaller than that observed by the previous group. However, the maximum AC voltage is only around 0.6 V which may be too low to overcome the forward bias of the rectifying bridge in order to convert AC to DC voltage.

In addition, Roundy et al. (2005) created prototyes of thin PZT structures with target volume power density of 80 $\mu W/cm^3$. Recently, duToit et al. (2005) and duToit & Wardle (2006) provided in-depth design principles for MEMS-scale piezoelectric energy harvesters and proposed a prototype of 30 $\mu W/cm^3$ from low-level vibration. Related issues on the modeling of miniaturized piezoelectric power harvesting devices include the works by duToit & Wardle (2007), Feng (2007), Horowitz et al. (2006), Lu et al. (2004), Prabhakar & Vengallatore (2007), Ramsay & Clark (2001), Trolier-Mckinstry & Muralt (2004), White et al. (2001), Xu et al. (2003), and Yeatman (2007).

3.1.3 Conversion Efficiency and Electrically Induced Damping

The efficiency of mechanical to electrical energy conversion is a fundamental parameter for the development and optimization of a power generation device. Umeda et al. (1996, 1997) have studied the efficiency of mechanical impact energy to electrical energy using a piezoelectric vibrator. Goldfarb & Jones (1999) subsequently investigated the efficiency of the piezoelectric material in a stack configuration for converting mechanical harmonic excitation into electrical energy. Roundy (2005) provided an expression for effectiveness that can be used to compare various approaches and designs for vibration-based energy harvesting devices (see also the work by Wang et al. (1999)). Recently, in contrast to efforts where the conversion efficiency was examined numerically (Umeda et al.1996), Richards et al. (2004) and Cho et al. (2006) derived an analytic formula to predict the energy conversion efficiency of piezoelectric energy harvesters in the case of AC power output. Since the electronic load requires a stabilized DC voltage while a vibrating piezoelectric element generates an AC voltage, the desired output needs to be rectified, filtered, and regulated to ensure the electric compatibility. Thus, Shu & Lien (2006b) investigated the conversion efficiency for a rectified piezoelectric power-harvesting system. They have shown that the conversion efficiency is dependent on the frequency ratio, the normalized resistance and, in particular, the ratio of electromechanical coupling coefficient to mechanical damping. In general, the conversion efficiency can be improved with a larger coupling coefficient and smaller damping. Recently, Cho et al. (2005a) and Cho et al. (2005b) performed a series of experiments and proposed a set of design guidelines for the performance optimization of micromachined piezoelectric membrane generators by enhancing the electromechanical coupling coefficient.

When an energy harvester is applied to a system, energy is removed from the vibrating structure and supplied to the desired electronic components, resulting in additional damping of the structure (Sodano et al. 2004). Because the efficiency is defined as the ratio of the time-averaged power dissipated across the load to that

done by the external force, electrically-induced damping can be defined explicitly. Lesieutre et al. (2004) have investigated the damping added to a structure due to the removal of electrical energy from the system during power harvesting. They have shown that the maximum induced electric damping corresponds to the optimal power transfer in the case of weak electromechanical coupling. However, unlike the work by Lesieutre et al. (2004), Shu & Lien (2006b) provided a new finding showing that the optimal electric load maximizing the conversion efficiency and induced electric damping is very different from that maximizing the harvested power in strongly coupled electromechanical systems. This shows that optimization criteria vary according to the relative strength of the coupling.

3.1.4 Power Storage Circuits

The research works cited above focus mainly on developing optimal energy-harvesting structures. However, the electrical outputs of these devices in many cases are too small to power electric devices directly. Thus, the methods of accumulating and storing parasitic energy are also the key to develop self-powered systems. Sodano et al. (2005a,b) have investigated several piezoelectric power-harvesting devices and the methods of accumulating energy by utilizing either a capacitor or a rechargeable battery. Ottman et al. (2002, 2003) have developed highly efficient electric circuits to store the generated charge or present it to the load circuit. They have claimed that at high levels of excitation, the power output can be increased by as much as 400%. In contrast to the linear load impedance adaptation by Ottman et al. (2002, 2003), Guyomar et al. (2005), Lefeuvre et al. (2005a,b) and Badel et al. (2006b) developed a new power flow optimization principle based on the technique, called *synchronized switch harvesting on inductor* (SSHI), for increasing the converted energy. They claimed that the electric harvested power may be increased by as much as 900% over the standard technique. Badel et al. (2005) subsequently extended to the case of pulsed excitation and Makihara et al. (2006) improved the SSHI technique by proposing a low-energy dissipation circuit. Recently, Shu et al. (2007) provided an improved analysis for the performance evaluation of a piezoelectric energy harvesting system using the SSHI electronic interface. They found that the best use of the SSHI harvesting circuit is for systems in the mid-range of electromechanical coupling. The degradation in harvested power due to the non-perfect voltage inversion is not pronounced in this case, and the reduction in power is much less sensitive to frequency deviations than that using the standard technique.

3.2 Approach

3.2.1 Standard AC–DC Harvesting Circuit

Consider an energy conversion device which includes a vibrating piezoelectric structure together with an energy storage system. If the modal density of such a

device is widely separated and the structure is vibrating at around its resonance frequency, we may model the power generator as a mass+spring+damper+piezo structure, as shown in Fig. 3.1 (Guyomar et al. 2005, Richards et al. 2004). It consists of a piezoelectric element coupled to a mechanical structure. In this approach, a forcing function $F(t)$ is applied to the system and an effective mass M is bounded on a spring of effective stiffness K, on a damper of coefficient η_{m}, and on a piezoelectric element characterized by effective piezoelectric coefficient Θ and capacitance C_{p}. These effective coefficients are dependent on the material constants and the design of energy harvesters and can be derived using the standard modal analysis (Hagood et al. 1990, Wang & Cross 1999).

For example, consider a triple-layer bender mounted as a cantilever beam with polarization poled along the thickness direction, as shown in Fig. 3.2. The electric field is generated through the direction of thickness of the piezoelectric layers, while strain is in the axial direction; consequently, the transverse, or $\{3\text{–}1\}$, mode is utilized. The effective coefficients related with material constants and structural geometry can be derived using the modal analysis (Shu & Lien 2006a).

$$
\begin{aligned}
M &= \beta_{\mathrm{M}}(m_{\mathrm{p}} + m_{\mathrm{b}}) + m_{\mathrm{a}},\\
K &= \beta_{\mathrm{K}}\, S \left\{ \left(\frac{2}{3}\frac{t^3}{L^3} + \frac{ht^2}{L^3} + \frac{1}{2}\frac{th^2}{L^3} \right) C^{\mathrm{E}}_{\mathrm{p}_{11}} + \frac{1}{12}\frac{h^3}{L^3} C^{\mathrm{E}}_{b_{11}} \right\},\\
\Theta &= \beta_{\Theta}\, \frac{S(h+t)}{2L} e_{31},\\
C_{\mathrm{p}} &= \frac{SL}{2t}\varepsilon^{S}_{33},
\end{aligned}
$$

where β_{M}, β_{K}, and β_{Θ} are constants derived from the Rayleigh–Ritz approximation, e_{31} and $\varepsilon^{\mathrm{S}}_{33}$ are the piezoelectric and clamped dielectric constants, respectively, S and

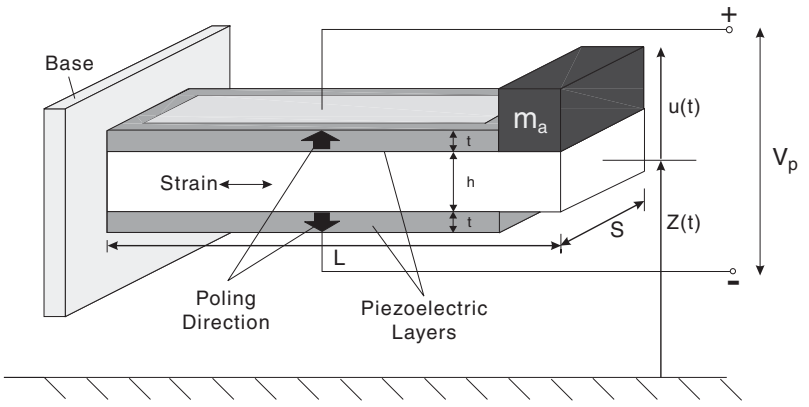

Fig. 3.2 A common piezoelectric-based power generator: a cantilever triple-layer bender operated in the $\{3\text{–}1\}$ mode. The base is excited with acceleration $\ddot{z}(t)$

L are the width and axial length of the cantilever beam, respectively, t and h, $C^{\mathrm{E}}_{p_{11}}$ and $C^{\mathrm{E}}_{b_{11}}$, m_{p} and m_{b} are the thicknesses, elastic moduli, and masses of the piezoelectric and central passive layers, and m_{a} is the attached mass. Another common piezoelectric power generator operated in the longitudinal or $\{3\text{–}3\}$ mode has been developed recently by Jeon et al. (2005) using interdigitated electrode configuration, as shown in Fig. 3.7. The advantage of utilizing this mode is that the longitudinal piezoelectric effect is usually much larger than the transverse effect ($d_{33} > d_{31}$).

Let u be the displacement of the mass M and V_{p} be the voltage across the piezoelectric element. The governing equations of the piezoelectric vibrator can be described by (Guyomar et al. 2005, Richards et al. 2004)

$$M\ddot{u}(t) + \eta_{\mathrm{m}}\dot{u}(t) + Ku(t) + \Theta V_{\mathrm{p}}(t) = F(t), \tag{3.1}$$

$$-\Theta\dot{u}(t) + C_{\mathrm{p}}\dot{V}_{\mathrm{p}}(t) = -I(t), \tag{3.2}$$

where $I(t)$ is the current flowing into the specified circuit as shown in Fig. 3.3. Since most applications of piezoelectric materials for power generation involve the use of periodic straining of piezoelectric elements, the vibrating generator is assumed to be driven at around resonance by the harmonic excitation

$$F(t) = F_0 \sin wt, \tag{3.3}$$

where F_0 is the constant magnitude and w (in radians per second) is the angular frequency of vibration.

The power generator considered here is connected to a storage circuit system, as shown in Fig. 3.1. Since the electrochemical battery needs a stabilized DC voltage while a vibrating piezoelectric element generates an AC voltage, this requires a suitable circuit to ensure the electric compatibility. Typically, an AC–DC rectifier followed by a filtering capacitance C_{e} is added to smooth the DC voltage, as shown in Fig. 3.1. A controller placed between the rectifier output and the battery is included to regulate the output voltage. Figure 3.3(a) is a simplified energy harvesting circuit commonly adopted for design analysis. It can be used to estimate an upper bound of the real power that the piezoelectric generator is able to deliver at a given excitation. Note that the regulation circuit and battery are replaced with an equivalent resistor R and V_{c} is the rectified voltage across it.

The common approach to have the stable output DC voltage is to assume that the filter capacitor C_{e} is large enough so that the rectified voltage V_{c} is essentially constant (Ottman et al. 2002). Specifically, $V_{\mathrm{c}}(t) = \langle V_{\mathrm{c}}(t)\rangle + V_{\mathrm{ripple}}$, where $\langle V_{\mathrm{c}}(t)\rangle$ and

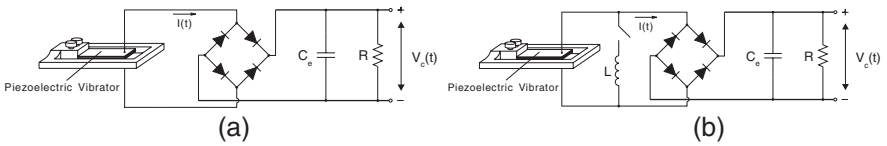

Fig. 3.3 (**a**) A standard energy harvesting circuit. (**b**) An SSHI energy harvesting circuit

V_{ripple} are the average and ripple of $V_c(t)$, respectively. This average $\langle V_c(t)\rangle$ is independent of C_e provided that the time constant RC_e is much larger than the oscillating period of the generator (Guyomar et al. 2005). The magnitude of V_{ripple}, however, depends on C_e and is negligible for large C_e. Under this hypothesis, $V_c(t) \approx \langle V_c(t)\rangle$, and therefore in the following, we use V_c, instead of $\langle V_c(t)\rangle$, to represent the average of $V_c(t)$ for notation simplicity.

The rectifying bridge shown in Fig. 3.3 is assumed to be perfect here. Thus, it is open circuited if the piezovoltage $|V_p|$ is smaller than the rectified voltage V_c. As a result, the current flowing into the circuit vanishes, and this implies $\dot{V}_p(t)$ varies proportionally with respect to $\dot{u}(t)$ as seen from (3.2). On the other hand, when $|V_p|$ reaches V_c, the bridge conducts and the piezovoltage is kept equal to the rectified voltage; i.e., $|V_p| = V_c$. Finally, the conduction in the rectifier diodes is blocked again when the absolute value of the piezovoltage $|V_p(t)|$ starts decreasing. Hence, the piezoelectric voltage $V_p(t)$ either varies proportionally with the displacement $u(t)$ when the rectifying bridge is blocking, or is kept equal to V_c when the bridge conducts.

The model equations (3.1, 3.2 and 3.3) are developed at the resonance mode of the device, and therefore, a single-mode vibration of the structure at the steady-state operation is expected with

$$u(t) = u_0 \sin(wt - \theta), \tag{3.4}$$

where u_0 is the magnitude and θ is the phase shift. This assumption of choosing the sinusoidal form for displacement has been made by Guyomar et al. (2005) excluding the effect of the phase shift θ. Shu & Lien (2006a) have included this effect and validated it both numerically and experimentally for the standard interface. The corresponding waveforms of $u(t)$ and $V_p(t)$ are shown in Fig. 3.4(a). Let $T = \frac{2\pi}{w}$ be the period of vibration, and t_i and t_f be two time instants ($t_f - t_i = \frac{T}{2}$) such that the displacement u undergoes from the minimum $-u_0$ to the maximum u_0, as shown in Fig. 3.4(a). Assumed that $\dot{V}_p \geq 0$ during the semi-period from t_i to t_f. It follows that $\int_{t_i}^{t_f} \dot{V}_p(t)\mathrm{d}t = V_c - (-V_c) = 2V_c$. Note that $C_e\dot{V}_c(t) + \frac{V_c}{R} = 0$ for $t_i < t < t^*$ during which the piezovoltage $|V_p| < V_c$ and $I(t) = C_e\dot{V}_c(t) + \frac{V_c}{R}$ for $t^* \leq t < t_f$ during which the rectifier conducts. This gives

$$-\int_{t_i}^{t_f} I(t)\mathrm{d}t = -\frac{T}{2}\frac{V_c}{R}$$

since the average current flowing through the capacitance C_e is zero; i.e., $\int_{t_i}^{t_f} C_e\dot{V}_c(t)\mathrm{d}t = 0$ at the steady-state operation. The integration of (3.2) from time t_i to t_f is therefore

$$-2\Theta u_0 + 2C_pV_c = -\frac{T}{2}\frac{V_c}{R},$$

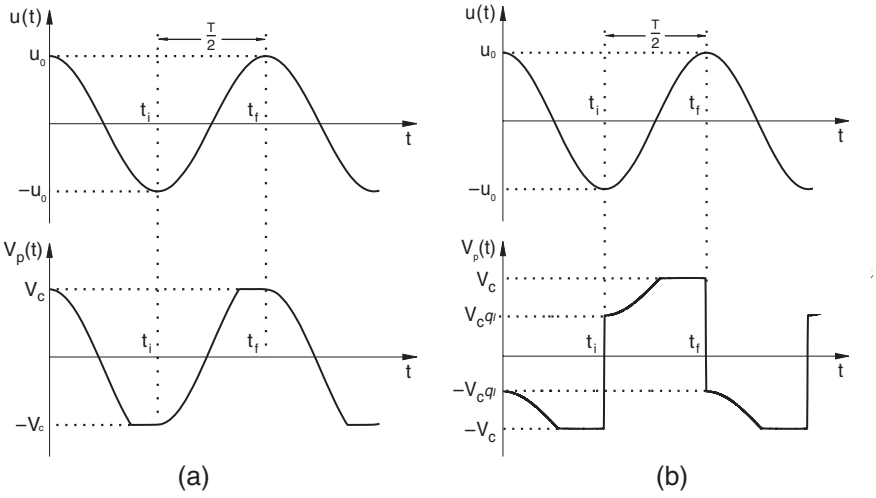

Fig. 3.4 Typical waveforms of displacement and piezoelectric voltage for (**a**) the standard and (**b**) the SSHI electronic interfaces

or

$$V_{\mathrm{c}} = \frac{w\Theta R}{wC_{\mathrm{p}}R + \frac{\pi}{2}}\, u_0. \tag{3.5}$$

Thus, from (3.5), u_0 has to be determined to decide V_{c}. There are three approaches in the recent literature for estimating it (Guyomar et al. 2005, Ottman et al. 2002, Shu & Lien 2006a). The first one models the piezoelectric device as the current source in parallel with its internal parasitic capacitance C_{p} (Jeon et al. 2005, Ng & Liao 2005, Ottman et al. 2002). It is based on the assumption that the internal current source of the generator is independent of the external load impedance. However, the amplitude of the current source is closely related to that of displacement which depends not only on the mechanical damping but also on the electrical damping at the resonant vibration (Lesieutre et al. 2004, Shu & Lien 2006b). This assumption is, therefore, not suitable when the effect of the electrical damping is significant. As a result, Guyomar et al. (2005) have proposed another estimation accounting for the effect of electromechanical coupling. Their estimation is based on the assumption that the external forcing function and the velocity of the mass are in-phase, or in other words, the phase shift effect is neglected in (3.4). Instead, Shu & Lien (2006a) have included this phase factor in their improved analysis, and derived the analytic expressions of displacement magnitude u_0, rectified voltage V_{c}, and harvested average power P. Their results are summarized as follows:

$$\overline{u}_0 = \frac{u_0}{\frac{F_0}{K}} = \frac{1}{\left\{\left(2\zeta_{\mathrm{m}} + \frac{2k_{\mathrm{e}}^2 r}{(r\Omega+\frac{\pi}{2})^2}\right)^2 \Omega^2 + \left(1 - \Omega^2 + \frac{k_{\mathrm{e}}^2 r\Omega}{r\Omega+\frac{\pi}{2}}\right)^2\right\}^{\frac{1}{2}}}, \tag{3.6}$$

$$\overline{V}_{\mathrm{c}} = \frac{V_{\mathrm{c}}}{\frac{F_0}{\Theta}} = \left(\frac{r\Omega}{r\Omega + \frac{\pi}{2}}\right) \frac{k_{\mathrm{e}}^2}{\left\{\left(2\zeta_{\mathrm{m}} + \frac{2k_{\mathrm{e}}^2 r}{(r\Omega+\frac{\pi}{2})^2}\right)^2 \Omega^2 + \left(1 - \Omega^2 + \frac{k_{\mathrm{e}}^2 r\Omega}{r\Omega+\frac{\pi}{2}}\right)^2\right\}^{\frac{1}{2}}}, \quad (3.7)$$

$$\overline{P} = \frac{P}{\frac{F_0^2}{w_{\mathrm{sc}} M}} = \frac{1}{\left(r\Omega + \frac{\pi}{2}\right)^2} \frac{k_e^2 \Omega^2 r}{\left\{\left(2\zeta_{\mathrm{m}} + \frac{2k_{\mathrm{e}}^2 r}{(r\Omega+\frac{\pi}{2})^2}\right)^2 \Omega^2 + \left(1 - \Omega^2 + \frac{k_{\mathrm{e}}^2 r\Omega}{r\Omega+\frac{\pi}{2}}\right)^2\right\}}, \quad (3.8)$$

where several dimensionless variables are introduced by

$$k_{\mathrm{e}}^2 = \frac{\Theta^2}{K C_{\mathrm{p}}}, \quad \zeta_{\mathrm{m}} = \frac{\eta_{\mathrm{m}}}{2\sqrt{K M}}, \quad w_{\mathrm{sc}} = \sqrt{\frac{K}{M}}, \quad \Omega = \frac{w}{w_{\mathrm{sc}}}, \quad r = C_{\mathrm{p}} w_{\mathrm{sc}} R. \quad (3.9)$$

Above k_{e}^2 is the alternative electromechanical coupling coefficient, ζ_{m} is the mechanical damping ratio, w_{sc} is the natural oscillation frequency (of the piezoelectric vibrator under the short circuit condition), Ω and r are the normalized frequency and electric resistance, respectively. Note that there are two resonances for the system since the piezoelectric structure exhibits both short-circuit and open-circuit stiffness. They are defined by

$$\Omega_{\mathrm{sc}} = 1, \quad \Omega_{\mathrm{oc}} = \sqrt{1 + k_{\mathrm{e}}^2}, \quad (3.10)$$

where Ω_{sc} and Ω_{oc} are the frequency ratios of short- and open-circuits, respectively. The shift in device natural frequency is pronounced if the coupling factor k_{e}^2 is large.

3.2.2 SSHI-Harvesting Circuit

An SSHI electronic interface consists of adding up a switch and an inductance L connected in series and is in parallel with the piezoelectric element, as shown in Fig. 3.3(b). The electronic switch is triggered according to the maximum and minimum of the displacement of the mass, causing the processing of piezoelectric voltage to be synchronized with the extreme values of displacement.

To illustrate the electrical behavior of this nonlinear processing circuit, consider the harmonic excitation given by (3.3). In view of the single-mode excitation, the mechanical displacement $u(t)$ is assumed to be sinusoidal as in (3.4) in steady-state operation. The validation of this assumption has been examined by considering the output voltage (Shu et al. 2007). The waveform of the piezoelectric voltage $V_{\mathrm{p}}(t)$, however, may not be sinusoidal and is dependent on the specific type of the interface circuit connected to the piezoelectric element. To see it, let $T = \frac{2\pi}{w}$ be the period of mechanical excitation and t_{i} and t_{f} be two time instants such that the displacement $u(t)$ undergoes from the minimum $-u_0$ to the maximum u_0, as illustrated in Fig. 3.4(b). The switch is turned off most of time during this semi-period $(t_{\mathrm{i}}^+, t_{\mathrm{f}})$. When it is turned on at the time instant t_{i}, $|V_p(t)|$ remains lower than the

rectified voltage V_c. So the rectifying bridge is open circuited, and an oscillating electrical circuit composed by the inductance L and the piezoelectric capacitance C_p is established, giving rise to an inversion process for the piezoelectric voltage V_p. Specifically, let Δt be the half electric period of this oscillating L-C_p circuit. It is equal to (Guyomar et al. 2005).

$$\Delta t = \pi\sqrt{LC_p}.$$

We assume that the inversion process is quasi-instantaneous in the sense that the inversion time is chosen to be much smaller than the period of mechanical vibration; i.e., $\Delta t = t_i^+ - t_i << T$. The switch is kept closed during this small time period Δt, resulting in the reverse of voltage on the piezoelectric element; i.e.,

$$V_p(t_i^+) = -V_p(t_i)e^{\frac{-\pi}{2Q_I}} = V_c q_I, \quad q_I = e^{\frac{-\pi}{2Q_I}}, \tag{3.11}$$

as shown in Fig. 3.4(b). Above Q_I is the inversion quality factor due to the energy loss mainly from the inductor in series with the switch. As a result, the current outgoing from the piezoelectric element through the rectifier during a half vibration period can be obtained by integrating (3.2) from time t_i^+ to t_f

$$\int_{t_i^+}^{t_f} \left\{-\Theta\dot{u}(t) + C_p\dot{V}_p(t)\right\} dt = -2\Theta u_0 + C_p\left(1 - e^{-\frac{\pi}{2Q_I}}\right)V_c = -\frac{T}{2}\frac{V_c}{R},$$

since the rectifier bridge is blocking during the inversion process and the inversion time $\Delta t << T$. The relation between the magnitude of displacement u_0 and the rectified voltage V_c is therefore obtained by

$$V_c = \frac{2R\Theta w}{(1-q_I)C_p R w + \pi}\, u_0. \tag{3.12}$$

The rest of the derivation is to estimate the magnitude of displacement u_0 and the phase shift θ, and we refer to the work by Shu et al. (2007) for details. The results for normalized displacement magnitude $\overline{u}_0^{\text{SSHI}}$, rectified voltage $\overline{V}_c^{\text{SSHI}}$, and average-harvested power $\overline{P}^{\text{SSHI}}$ are given, respectively, by

$$\begin{aligned}\overline{u}_0^{\text{SSHI}} &= \frac{u_0^{\text{SSHI}}}{\frac{F_0}{K}} \\ &= \frac{1}{\left\{\left(2\zeta_m + \frac{2\left[1+\frac{r\Omega}{2\pi}(1-q_I^2)\right]k_c^2 r}{\left(\frac{(1-q_I)}{2}r\Omega+\frac{\pi}{2}\right)^2}\right)^2\Omega^2 + \left(1-\Omega^2+\frac{\frac{(1-q_I)}{2}k_c^2 r\Omega}{\frac{(1-q_I)}{2}r\Omega+\frac{\pi}{2}}\right)^2\right\}^{\frac{1}{2}}},\end{aligned} \tag{3.13}$$

$$\begin{aligned}\overline{V}_{\mathrm{c}}^{\mathrm{SSHI}} &= \frac{V_{\mathrm{c}}^{\mathrm{SSHI}}}{\frac{F_0}{\Theta}} \\ &= \left(\frac{r\Omega}{\frac{(1-q_1)}{2}r\Omega+\frac{\pi}{2}}\right) \\ &\quad \times \frac{k_e^2}{\left\{\left(2\zeta_{\mathrm{m}}+\frac{2\left[1+\frac{r\Omega}{2\pi}(1-q_{\mathrm{I}}^2)\right]k_{\mathrm{e}}^2 r}{\left(\frac{(1-q_1)}{2}r\Omega+\frac{\pi}{2}\right)^2}\right)^2\Omega^2+\left(1-\Omega^2+\frac{\frac{(1-q_1)}{2}k_{\mathrm{e}}^2 r\Omega}{\frac{(1-q_1)}{2}r\Omega+\frac{\pi}{2}}\right)^2\right\}^{\frac{1}{2}}}, \quad (3.14)\end{aligned}$$

$$\begin{aligned}\overline{P}^{\mathrm{SSHI}} &= \frac{P^{\mathrm{SSHI}}}{\frac{F_0^2}{w_{\mathrm{sc}}M}} \\ &= \left(\frac{1}{\frac{(1-q_1)}{2}r\Omega+\frac{\pi}{2}}\right)^2 \\ &\quad \times \frac{k_e^2\Omega^2 r}{\left(2\zeta_{\mathrm{m}}+\frac{2\left[1+\frac{r\Omega}{2\pi}(1-q_{\mathrm{I}}^2)\right]k_{\mathrm{e}}^2 r}{\left(\frac{(1-q_1)}{2}r\Omega+\frac{\pi}{2}\right)^2}\right)^2\Omega^2+\left(1-\Omega^2+\frac{\frac{(1-q_1)}{2}k_{\mathrm{e}}^2 r\Omega}{\frac{(1-q_1)}{2}r\Omega+\frac{\pi}{2}}\right)^2}. \quad (3.15)\end{aligned}$$

Above all are expressed in terms of dimensionless parameters defined in (3.9) and (3.11).

Finally, Guyomar et al. (2005) have used the in-phase assumption to analyze the electrical performance of the power generator using the SSHI interface. To be precise, they have assumed that the external forcing function and the velocity of the mass are in-phase, giving rise to no phase shift effect in their formulation. The following summaries their results for comparisons:

$$\overline{u}_{\text{in-phase}}^{\mathrm{SSHI}} = \frac{u_{\text{in-phase}}^{\mathrm{SSHI}}}{\frac{F_0}{K}} = \frac{1}{\left\{2\zeta_{\mathrm{m}}+\frac{2\left[1+\frac{r\Omega}{2\pi}(1-q_{\mathrm{I}}^2)\right]k_{\mathrm{e}}^2 r}{\left(\frac{(1-q_1)}{2}r\Omega+\frac{\pi}{2}\right)^2}\right\}\Omega}, \quad (3.16)$$

$$\overline{V}_{\text{in-phase}}^{\mathrm{SSHI}} = \frac{V_{\text{in-phase}}^{\mathrm{SSHI}}}{\frac{F_0}{\Theta}} = \left(\frac{r}{\frac{(1-q_1)}{2}r\Omega+\frac{\pi}{2}}\right)\frac{k_e^2}{\left\{2\zeta_{\mathrm{m}}+\frac{2\left[1+\frac{r\Omega}{2\pi}(1-q_{\mathrm{I}}^2)\right]k_{\mathrm{e}}^2 r}{\left(\frac{(1-q_1)}{2}r\Omega+\frac{\pi}{2}\right)^2}\right\}}, \quad (3.17)$$

$$\overline{P}_{\text{in-phase}}^{\mathrm{SSHI}} = \frac{P_{\text{in-phase}}^{\mathrm{SSHI}}}{\frac{F_0^2}{w_{\mathrm{sc}}M}} = \frac{1}{\left(\frac{(1-q_1)}{2}r\Omega+\frac{\pi}{2}\right)^2}\frac{k_{\mathrm{e}}^2 r}{\left\{2\zeta_{\mathrm{m}}+\frac{2\left[1+\frac{r\Omega}{2\pi}(1-q_{\mathrm{I}}^2)\right]k_{\mathrm{e}}^2 r}{\left(\frac{(1-q_1)}{2}r\Omega+\frac{\pi}{2}\right)^2}\right\}^2}. \quad (3.18)$$

3.3 Results

3.3.1 Standard Interface

The improved estimates in (3.6, 3.7 and 3.8) for the standard AC–DC interface have been found to agree well with experimental observations and numerical simulations of (3.1) and (3.2) under (3.3) (Shu & Lien 2006a). Therefore, these estimates are suitable for the electrical performance evaluation of the piezoelectric energy harvesting system embedded with the standard electronic interface. Basically from (3.8), the harvested average power increases significantly for smaller mechanical damping ratio ζ_m or larger electromechanical coupling coefficient k_e^2. It is consistent with that found by (Badel et al. 2006a), who have performed an interesting experiment by comparing the performances of vibration-based piezoelectric power generators using a piezoelectric ceramic and a single crystal. Under the same operating condition, the power generated using the single crystal is much higher than that using the ceramic, since according to their measurements the coupling factor k_e^2 of the former is 20 times larger than that of the latter. However, one has to be cautious that the average-harvested power approaches to its saturation value for much larger k_e^2, as shown in Fig. 3.5.

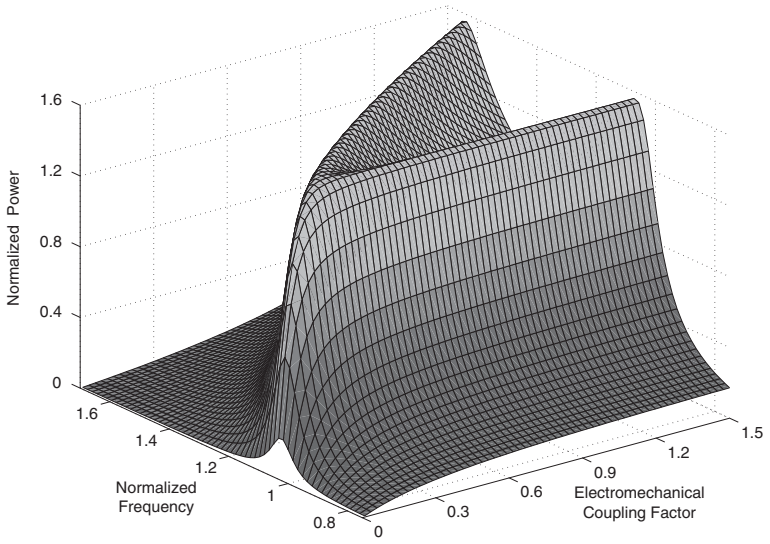

Fig. 3.5 The normalized power $\overline{P}$ against the normalized frequency Ω and the electromechanical coupling factor k_e^2 at the optimal condition in the sense that $\overline{P}^{\text{opt}}(\Omega, k_e^2, \zeta_m) = \overline{P}(r^{\text{opt}}(\Omega), \Omega, k_e^2, \zeta_m)$ and $r^{\text{opt}}(\Omega)$ is determined by solving $\frac{\partial}{\partial r}\overline{P}(r, \Omega, k_e^2, \zeta_m) = 0$. We use $\zeta_m = 0.04$ here. Note that for large k_e^2 there are two identical peaks of power evaluated at the frequency ratio close to $\Omega_{sc} = 1$ and $\Omega_{oc} = \sqrt{1 + k_e^2}$. These peaks are saturated for much higher coupling factor $k_e^2 >> 1$ (Shu et al. 2007)

The improved estimates in (3.6, 3.7 and 3.8) have also been compared with the uncoupled and in-phase estimates according to the relative magnitudes of electromechanical coupling coefficient and mechanical damping ratio. The results given by Shu & Lien (2006a) show that the conventional uncoupled solutions and in-phase estimates are suitable, provided that the ratio $\frac{k_e^2}{\zeta_m} << 1$, while the discrepancies among these distinct approaches become significant when $\frac{k_e^2}{\zeta_m}$ increases. If the shift in device natural frequency is pronounced and the mechanical damping ratio of the system is small; i.e. $\frac{k_e^2}{\zeta_m} >> 1$, the harvested power is shown to have two optimums evaluated at $(r_1^{opt}, \Omega_1^{opt})$ and $(r_2^{opt}, \Omega_2^{opt})$, where Ω_1^{opt} is close to Ω_{sc} and the electric load r_1^{opt} is very small, while Ω_2^{opt} is close to Ω_{oc} and r_2^{opt} is large. Indeed, Table 3.1 summarizes the relationship between the system parameters k_e^2 and ζ_m and the normalized load, displacement, voltage, and power at these two optimal conditions. The first optimal pair is designed at the short-circuit resonance Ω_{sc} with the optimal

Table 3.1 The relation between the system parameters k_e^2 and ζ_m and the normalized electric resistance, displacement, voltage, and power operated at the short-circuit (Ω_{sc}) and open-circuit (Ω_{oc}) resonances (Shu & Lien 2006a). Note that the condition $\frac{k_e^2}{\zeta_m} >> 1$ is implied in the analysis

Optimal conditions	Ω_{sc}		Ω_{oc}
Resistance	$r_{sc}^{opt} \propto \frac{1}{\frac{k_e^2}{\zeta_m}}$	$<$	$r_{oc}^{opt} \propto \frac{1}{(1+k_e^2)} \frac{k_e^2}{\zeta_m}$
Displacement	$\overline{u}_0^{opt} \propto \frac{1}{\zeta_m}$	$>$	$\overline{u}_0^{opt} \propto \frac{1}{\zeta_m(\sqrt{1+k_e^2})}$
Voltage	$\overline{V}_c^{opt} \propto 1$	$<$	$\overline{V}_c^{opt} \propto \frac{1}{\sqrt{1+k_e^2}} \frac{k_e^2}{\zeta_m}$
Power	$\overline{P}^{opt} \propto \frac{1}{\zeta_m}$	$=$	$\overline{P}^{opt} \propto \frac{1}{\zeta_m}$

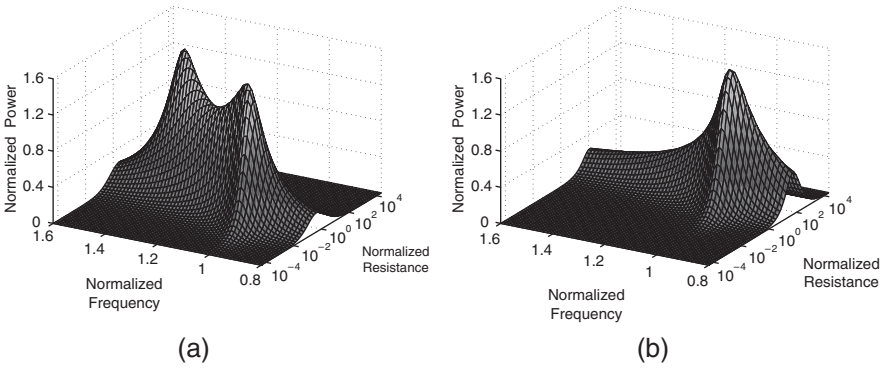

Fig. 3.6 The normalized power against the normalized electric resistance and frequency ratio. (**a**) A strongly coupled electromechanical system using the standard AC/DC electronic interface ($k_e^2 = 1.0$, $\zeta_m = 0.04$ $\frac{k_e^2}{\zeta_m} = 25$). (**b**) A weakly coupled electromechanical system using the ideal SSHI electronic interface ($k_e^2 = 0.01$, $\zeta_m = 0.04$, $\frac{k_e^2}{\zeta_m} = 0.25$, $Q_I = \infty$). Notice that both (a) and (b) provide the identical peaks of harvested power evaluated at different conditions (Shu et al. 2007)

load $r_{\mathrm{sc}}^{\mathrm{opt}} \propto \frac{1}{\frac{k_{\mathrm{e}}^2}{\zeta_{\mathrm{m}}}}$, while the second one is designed at the open-circuit resonance Ω_{oc} with the optimal load $r_{\mathrm{oc}}^{\mathrm{opt}} \propto \frac{1}{(1+k_{\mathrm{e}}^2)} \frac{k_{\mathrm{e}}^2}{\zeta_{\mathrm{m}}}$. They give the identical value of maximum harvested power which depends only on the mechanical damping ratio ζ_{m}. Unlike the power, the displacement is higher at Ω_{sc} than at Ω_{oc}, while the voltage operating at the first peak is one order of magnitude smaller than that operating at the second peak.

Figure 3.6(a) gives the dependence of the normalized harvested power on the normalized resistance and frequency ratio for the case of strong electromechanical coupling. While such a strong coupling is not commonly observed in the conventional piezoelectric power generators, we particularly emphasize it here since it has been shown by Shu et al. (2007) that the behavior of an ideal SSHI system is similar to that of a strongly coupled electromechanical standard system excited at around the short-circuit resonance. This finding is generally valid no matter whether the real electromechanical system is weakly or strongly coupled.

Discussions

If the vibration source is due to the periodic excitation of some base, this gives $F_0 = MA$ where A is the magnitude of acceleration of the exciting base. From (3.8), the harvested average power per unit mass becomes

$$\frac{P}{M} = \frac{A^2}{w_{\mathrm{sc}}} \overline{P}(r, \Omega, k_{\mathrm{e}}^2, \zeta_{\mathrm{m}}). \tag{3.19}$$

As (3.19) is expressed in terms of a number of dimensionless parameters, an effective power normalization scheme is provided and can be used to compare power-harvesting devices of various sizes and with different vibration inputs to estimate efficiencies. Conceptually, the formula (3.19) provides a design guideline to optimize AC–DC power output either by tuning the electric resistance, selecting suitable operation points, or by adjusting the coupling coefficient by careful structural design. However, it needs much more efforts to make this scheme feasible due to the following various reasons.

(a) It may not be an easy task to adjust one parameter with other parameters fixed. For example, adjusting the dimensions of the device may result in the simultaneous changes of the whole dimensionless parameters r, Ω, k_{e}^2, and ζ_{m}.
(b) Current design requires that the natural frequency of the device is below 300 Hz since a number of common ambient sources have significant vibration components in the frequency range of 100–300 Hz (duToit et al. 2005). This adds a constraint for optimizing (3.19). Moreover, the most common geometry for piezoelectric power generators is the cantilever beam configuration. It is well known that its first resonance is proportional to the inverse of the beam length, causing the pronounced increase of natural frequency at the microscale. For example, the

resonance frequency of the MEMS-based piezoelectric micro power generator developed by MIT has been measured as high as 13.9 kHz (Jeon et al. 2005). However, this order of magnitude of 10 kHz frequency is not low enough to meet the frequency range of common ambient sources, neither high enough to match that of supersonic transducers, for example.

(c) Operating the piezoelectric element in the $\{3\text{–}3\}$ actuation mode is advantageous since better coupling between the mechanical and the electrical domain is possible ($d_{33} > d_{31}$ in general). Conventionally, longitudinal mode operation occurs through the use of interdigitated electrodes, as shown in Fig. 3.7, since a large component of the electric field can be produced in the axial direction. Based on this design, Jeon et al. (2005) have successfully developed the first MEMS-based piezoelectric power generator and found a maximum DC voltage of 3 V across the load 10.1 MΩ. However, another very recent paper in 2006 by Sodano et al. (2006) have observed the poor performance of bulk energy harvester with interdigitated electrode configuration. The reasons for these two seemingly contradictory experiments are not clear. One possible explanation is that the generated electric field decays significantly far away from the interdigitated electrode surface, causing the degradation of performance for bulk generators.

(d) In general, the harvested average power arises as the electromechanical coupling coefficient ascends at the early stage, as can be seen from Fig. 3.5. One proposed method to increase the coupling coefficient k_e^2 is to apply destabilizing axial loads, as shown in Fig. 3.8 (Lesieutre & Davis 1997). The idea behind it is that the beam's apparent stiffness is the function of the axial compressive preload; it theoretically reduces to zero as the axial preload approaches the critical bucking load. Using this idea, Leland & Wright (2006) have observed the coupling coefficient rising as much as 25%. However, the device damping also rises 67% which is not favorable for improving harvested power extraction. Hence, it needs more quantitative efforts to investigate this idea and therefore, to find out the suitable trade-off relationship (see also a recent investigation by Hu et al. (2007b)).

(e) Vibration-based power generators achieve the maximum power when their resonance frequency matches the driving frequency. However, the scavengeable power decreases significantly and almost goes away if the frequency deviation is more than 5% from the resonant frequency (Charnegie et al. 2006, Muriuki & Clark 2007, Shahruz 2006). Due to inconsistencies in the fabrication of the

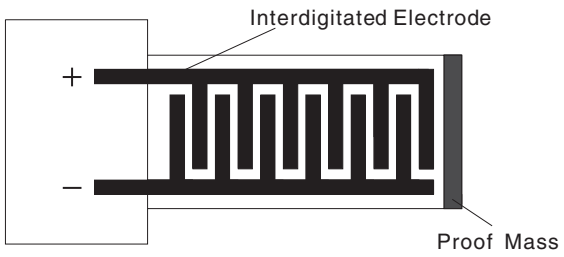

Fig. 3.7 An interdigitated electrode configuration

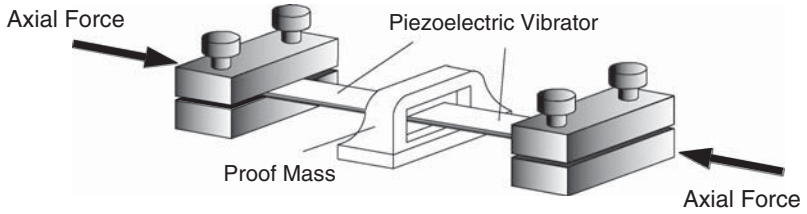

Fig. 3.8 The beam stiffness is able to be reduced by applying destabilizing compressive preloads

harvester or variations in the source, frequency matching can be difficult to achieve. Thus, it is obviously advantageous to have a single design operating effectively over a range of vibration frequencies, and Roundy et al. (2005) have suggested to use multi-mass and multi-mode resonators to enlarge the bandwidth of generators. In addition, Challa et al. (2008) have used a magnetic force technique to develop a resonance frequency tunable energy harvesting device.

(f) Note that (3.19) is an estimation of an upper bound of the real power that a piezoelectric energy harvester is able to deliver at a given excitation. Thus, research on power circuit designs can be viewed as efforts to improve the actual power extraction (but cannot increase its maximum power). The most common circuit design is to use the principle of load impedance adaptation by tuning the load impedance to achieve the higher power flow (Ottman et al. 2003). Guyomar and co-workers (Badel et al. 2006a, Badel et al. 2005, Guyomar et al. 2005, Lefeuvre et al. 2005b, 2006) have developed another new technique (SSHI) for increasing the converted energy, which has been discussed in Section 3.2.2. Recently, Liu et al. (2007) have investigated the electromechanical conversion capacity of a piezoelectric power generator by considering a quasi-static work cycle, and pointed out theoretically that their proposed method yields more power than SSHI.

3.3.2 SSHI Interface

The in-phase estimates in (3.16), (3.17) and (3.18) provided by Guyomar et al. (2005) are lack of frequency dependence. Thus, they are unable to predict the system behavior when the applied driving frequency deviates from the system resonance frequency. As the reduction in power is significant due to frequency deviation, such an effect cannot be ignored in practical design. The improved estimates in (3.13), (3.14) and (3.15) for the SSHI interface, on the other hand, exhibit the frequency dependence, and have also been validated numerically by Shu et al. (2007). Therefore, these estimates are suitable for the electrical performance evaluation of the piezoelectric energy harvesting system embedded with an SSHI interface circuit.

To see how the SSHI electronic interface boosts power extraction, consider an ideal case where the inversion of the piezoelectric voltage V_p is complete; i.e., $Q_I = \infty$. From (3.11) this gives $q_I = 1$ and the normalized harvested power from (3.15) becomes

$$\overline{P}^{\mathrm{SSHI}} = \frac{4}{\pi^2} \frac{r k_{\mathrm{e}}^2 \Omega^2}{\left\{ 4 \left(\zeta_{\mathrm{m}} + \frac{4 k_{\mathrm{e}}^2 r}{\pi^2} \right)^2 \Omega^2 + (1 - \Omega^2)^2 \right\}}. \tag{3.20}$$

The optimal electric load resistance and the normalized power operated at Ω_{sc} are therefore

$$r^{\mathrm{opt}} = \frac{\pi^2}{4} \frac{1}{\frac{k_{\mathrm{e}}^2}{\zeta_{\mathrm{m}}}}, \quad \overline{P}^{\mathrm{SSHI}}|_{r=r^{\mathrm{opt}},\, \Omega=1} = \frac{1}{16\zeta_{\mathrm{m}}}. \tag{3.21}$$

From (3.21), the optimal load resistance is inversely proportional to the ratio $\frac{k_{\mathrm{e}}^2}{\zeta_{\mathrm{m}}}$, while the corresponding optimal power depends only on the mechanical damping ratio ζ_{m} and is independent of the electromechanical coupling coefficient k_{e}^2. Comparing all of these features with Table 3.1 suggests that the behavior of the power-harvesting system using the SSHI interface is similar to that of a strongly coupled electromechanical system using the standard interface and operated at the short-circuit resonance Ω_{sc}. In addition, according to Table 3.1, there exists another identical peak of power operated at the open-circuit resonance. But Shu et al. (2007) have also shown that the second peak of power is moved to the infinite point in the (r, Ω) space, and therefore, there is only one peak of power for the SSHI electronic interface no matter whether the real electromechanical system is weakly or strongly coupled, as schematically shown in Fig. 3.6(b). Note that we particularly take $k_{\mathrm{e}}^2 = 0.01$ and $\zeta_{\mathrm{m}} = 0.04$ in Fig. 3.6(b) so that the electromechanical generator itself is weakly coupled $\left(\frac{k_{\mathrm{e}}^2}{\zeta_{\mathrm{m}}} = 0.25 \right)$. The harvested power obtained using the standard harvesting circuit is pretty small in this case, since it has been shown that (Shu & Lien 2006a)

$$\overline{P}\left(r^{\mathrm{opt}} = \frac{\pi}{2}, \Omega = 1, k_{\mathrm{e}}^2, \zeta_{\mathrm{m}} \right) \approx \left(\frac{2}{\pi} \frac{k_{\mathrm{e}}^2}{\zeta_{\mathrm{m}}} \right) \frac{1}{16\zeta_{\mathrm{m}}} << \frac{1}{16\zeta_{\mathrm{m}}} = \left(\overline{P}^{\mathrm{SSHI}} \right)_{\max}$$

if $\frac{k_{\mathrm{e}}^2}{\zeta_{\mathrm{m}}} << 1$. But the inclusion of SSHI circuit boosts the average harvested power whose maximum is the same as that using a strongly coupled electromechanical generator connected to the standard interface, as illustrated in Fig. 3.6(a) ($k_{\mathrm{e}}^2 = 1.0$, $\zeta_{\mathrm{m}} = 0.04$ and $\frac{k_{\mathrm{e}}^2}{\zeta_{\mathrm{m}}} = 25$). Therefore, the harvested power increases tremendously for any weak coupling SSHI system at the cost of using a much larger optimal electric load which is proportional to $\frac{1}{\frac{k_{\mathrm{e}}^2}{\zeta_{\mathrm{m}}}}$ according to (3.21).

As in many practical situations, the inversion of the piezoelectric voltage V_{p} is not perfect ($Q_{\mathrm{I}} \neq \infty$), which accounts for a certain amount of the performance degradation using the SSHI electronic interface. We take $Q_{\mathrm{I}} = 2.6$ for the comparisons of the electrical performance of a vibration-based piezoelectric power generator using the standard and SSHI electronic interfaces according to the different ratios of $\frac{k_{\mathrm{e}}^2}{\zeta_{\mathrm{m}}}$. The results are shown in Fig. 3.9 (Shu et al. 2007). Note that it is possible to have

a larger value of quality factor Q_1 by requiring the use of the low losses inductor (Lefeuvre et al. 2006).

To explain Fig. 3.9, first consider a weakly coupled electromechanical system; i.e., the ratio $\frac{k_e^2}{\zeta_m} << 1$. We take $k_e^2 = 0.01$ and $\zeta_m = 0.04$ for demonstration. This gives $\frac{k_e^2}{\zeta_m} = 0.25$. Comparing Fig. 3.9(a) with Fig. 3.9(d) gives the achieved optimal power using SSHI is three times larger than that using the standard interface ($\overline{P}^{\text{SSHI}}|_{Q_1=2.6} = 0.67$ and $\overline{P} = 0.23$). However, there is a significant performance degradation in this case since the maximum normalized power generated for the ideal voltage inversion is around $\overline{P}^{\text{SSHI}}|_{Q_1=\infty} = 1.56$.

Next, suppose the electromechanical coupling is in the medium range; i.e., the ratio of $\frac{k_e^2}{\zeta_m}$ is of order 1. We take $k_e^2 = 0.09$ and $\zeta_m = 0.04$. This gives $\frac{k_e^2}{\zeta_m} = 2.25$. Comparing Fig. 3.9(b) with Fig. 3.9(e) gives $\overline{P}^{\text{SSHI}}|_{Q_1=2.6} = 1.38$, the maximum normalized power for the non-ideal voltage inversion, and $\overline{P} = 1.20$, the maximum normalized power for the standard interface. While there is no significant increase of power output using the SSHI electronic interface in this case, Fig. 3.9(e) demonstrates that the harvested power evaluated at around the optimal load is less sensitive to frequency deviated from the resonant vibration. For example, the amount of normalized harvested power $\overline{P}$ evaluated at $r = \frac{\pi}{2}$ in the standard case drops from 1.2 to 0.6 for about 5% frequency deviation, and from 1.2 to 0.2 for about 10% frequency deviation. However, under the same conditions, the normalized harvested power $\overline{P}^{\text{SSHI}}$ in the SSHI circuit drops from 1.3 to only 1.0 for about 5% frequency deviation, and from 1.3 to 0.5 for about 10% frequency deviation. It has also been shown that this frequency-insensitive feature is much more pronounced if the quality factor Q_1 is further improved (Shu et al. 2007).

Finally, we turn to a strongly coupled electromechanical system $\left(\frac{k_e^2}{\zeta_m} >> 1\right)$. We take $k_e^2 = 1.0$ and $\zeta_m = 0.04$, and this gives $\frac{k_e^2}{\zeta_m} = 25$. The results are shown in Fig. 3.9(c) based on the standard interface and in Fig. 3.9(f) based on the SSHI interface. In the standard case, the harvested power has two identical optimal peaks, and the switching between these two peaks can be achieved by varying the electric loads. The envelope of these peaks has a local minimum, which is closely related to the minimum proof mass displacement. On the other hand, there is only one peak of power in the SSHI circuit, as explained previously. Unlike the standard case, as illustrated in Fig. 3.9(c), the peaks of the average harvested power decrease significantly as the load resistances increase, as shown in Fig. 3.9(f). In addition, it can be seen from (3.21) that the optimal electric load for the SSHI system is very small, since $\frac{k_e^2}{\zeta_m} >> 1$. Thus, Fig. 3.9(f) indicates that any deviation in the load resistance will cause a significant power drop in the SSHI case. Such an effect cannot be ignored in practical design, since there may exist other inherent electrical damping in the whole circuit system; for example, the diode loss is not taken into account in the present analysis. As a result, there seems to be no obvious advantage of using the SSHI electronic interface from the comparison between Fig. 3.9(c) and Fig. 3.9(f).

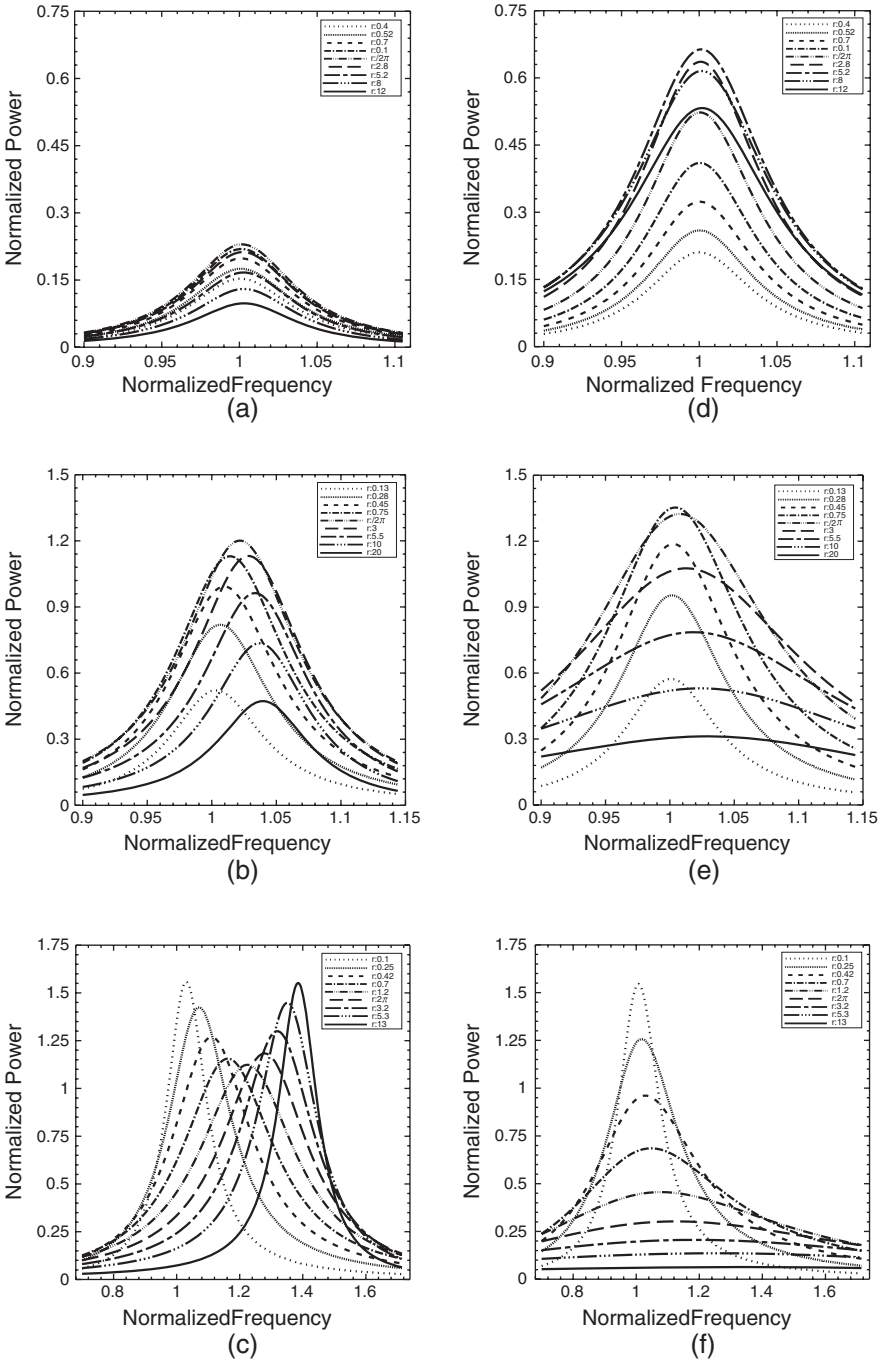

Fig. 3.9 Normalized power versus frequency ratio for different values of normalized resistances. Notice that (**a**)–(**c**) are obtained using the standard electronic interface, while (**d**)–(**f**) are obtained using the SSHI electronic interface (Shu et al. 2007)

3.4 Conclusion

This chapter presents a theory of piezoelectric vibration-based energy harvesting following the works by Shu & Lien (2006a), Shu & Lien (2006b) and Shu et al. (2007). The theory is able to predict the electrical behavior of piezoelectric power-harvesting systems using either the standard or the SSHI electronic interface. It shows that power extraction depends on the input vibration characteristics (frequency and acceleration), the mass of the generator, the electrical load, the natural frequency, the mechanical damping ratio, the electromechanical coupling coefficient of the system, and/or the inversion quality factor of an SSHI circuit. An expression of average harvested power incorporating all of these factors is analytically provided by (3.8) or (3.15) for the standard or SSHI interface. As the formula is expressed in terms of a number of dimensionless parameters, an effective power normalization scheme is provided and can be used to compare power harvesting devices of various sizes and with different vibration inputs to estimate efficiencies. Further, it is also highly recommended to provide all these parameters in all future publications to facilitate the relative comparison of various devices. Finally, the developed theory also points to opportunities for new devices and improvements in existing ones. For example, it shows that optimization criteria vary according to the relative strength of coupling, and scavenger bandwidth is improved by SSHI technique.

Acknowledgments The author is grateful to W. J. Wu and I. C. Lien for many pleasant collaborations and very helpful comments on this chapter. The author is glad to acknowledge the partial supports from National Science Council under Grant No. 96-2628-E-002-119-MY3, and from Ministry of Economic Affair under Grant No. 96-EC-17-A-05-S1-017 (WHAM-BioS).

References

Ajitsaria1, J., Choe, S. Y., Shen, D. and Kim, D. J. (2007). Modeling and Analysis of a Bimorph Piezoelectric Cantilever Beam for Voltage Generation, *Smart Materials and Structures* **16**: 447–454.

Allen, J. J. and Smits, A. J. (2001). Energy Harvesting EEL, *Journal of Fluids and Structures* **15**: 629–640.

Anton, S. R. and Sodano, H. A. (2007). A Review of Power Harvesting using Piezoelectric Materials (2003-2006), *Smart Materials and Structures* **16**: R1–R21.

Badel, A., Benayad, A., Lefeuvre, E., Lebrun, L., Richard, C. and Guyomar, D. (2006a). Single Crystals and Nonlinear Process for Outstanding Vibration-Powered Electrical Generators, *IEEE Transaction on Ultrasonics, Ferroelectrics, and Frequency Control* **53**: 673–684.

Badel, A., Guyomar, D., Lefeuvre, E. and Richard, C. (2005). Efficiency Enhancement of a Piezoelectric Energy Harvesting Device in Pulsed Operation by Synchronous Charge Inversion, *Journal of Intelligent Material Systems and Structures* **16**: 889–901.

Badel, A., Guyomar, D., Lefeuvre, E. and Richard, C. (2006b). Piezoelectric Energy Harvesting Using a Synchronized Switch Technique, *Journal of Intelligent Material Systems and Structures* **17**: 831–839.

Beeby, S. P., Torah, R. N., Tudor, M. J., Glynne-Jones, P., O'Donnell, T., Saha, C. R. and Roy, S. (2007). A Micro Electromagnetic Generator for Vibration Energy Harvesting, *Journal of Micromechanics and Microengineering* **17**: 1257–1265.

Brufau-Penella, J., Puig-Vidal, M., Giannone, P., Graziani, S. and Strazzeri, S. (2008). Characterization of the Harvesting Capabilities of an Ionic Polymer Metal Composite Device, *Smart Materials and Structures* **17**: 015009.

Challa, V. R., Prasad, M. G., Shi, Y. and Fisher, F. T. (2008). A Vibration Energy Harvesting Device with Bidirectional Resonance Frequency Tunability, *Smart Materials and Structures* **17**: 015035.

Chandrakasan, A., Amirtharajah, R., Goodman, J. and Rabiner, W. (1998). Trends in Low Power Digital Signal Processing, *International Symposium on Circuits and Systems* **4**: 604–607.

Charnegie, D., Mo, C., Frederick, A. A. and Clark, W. W. (2006). Tunable Piezoelectric Cantilever for Energy Harvesting, *Proceedings of 2006 ASME International Mechanical Engineering Congress and Exposition*, pp. IMECE2006–14431.

Cheng, S., Wang, N. and Arnold, D. P. (2007). Modeling of Magnetic Vibrational Energy Harvesters using Equivalent Circuit Representations, *Journal of Micromechanics and Microengineering* **17**: 2328–2335.

Cho, J., Anderson, M., Richards, R., Bahr, D. and Richards, C. (2005a). Optimization of Electromechanical Coupling for a Thin-Film PZT Membrane: I. Modeling, *Journal of Micromechanics and Microengineering* **15**: 1797–1803.

Cho, J., Anderson, M., Richards, R., Bahr, D. and Richards, C. (2005b). Optimization of Electromechanical Coupling for a Thin-Film PZT Membrane: II. Experiment, *Journal of Micromechanics and Microengineering* **15**: 1804–1809.

Cho, J. H., Richards, R. F., Bahr, D. F., Richards, C. D. and Anderson, M. J. (2006). Efficiency of Energy Conversion by Piezoelectrics, *Applied Physics Letter* **89**: 104107.

Choi, W. J., Jeon, Y., Jeong, J. H., Sood, R. and Kim, S. G. (2006). Energy Harvesting MEMS Device Based on Thin Film Piezoelectric Cantilevers, *Journal of Electroceramics* **17**: 543–548.

Cornwell, P. J., Goethal, J., Kowko, J. and Damianakis, M. (2005). Enhancing Power Harvesting Using a Tuned Auxiliary Structure, *Journal of Intelligent Material Systems and Structures* **16**: 825–834.

duToit, N. E. and Wardle, B. L. (2006). Performance of Microfabricated Piezoelectric Vibration Energy Harvesters, *Integrated Ferroelectrics* **83**: 13–32.

duToit, N. E. and Wardle, B. L. (2007). Experimental Verification of Models for Microfabricated Piezoelectric Vibration Energy Harvesters, *AIAA Journal* **45**: 1126–1137.

duToit, N. E., Wardle, B. L. and Kim, S. G. (2005). Design Considerations for MEMS-Scale Piezoelectric Mechanical Vibration Energy Harvesters, *Integrated Ferroelectrics* **71**: 121–160.

Elvin, N., Elvin, A. and Choi, D. H. (2003). A Self-Powered Damage Detection Sensor, *Journal of Strain Analysis* **38**: 115–124.

Elvin, N. G., Elvin, A. A. and Spector, M. (2001). A Self-Powered Mechanical Strain Energy Sensor, *Smart Materials and Structures* **10**: 293–299.

Elvin, N. G., Lajnef, N. and Elvin, A. A. (2006). Feasibility of Structural Monitoring with Vibration Powered Sensors, *Smart Materials and Structures* **15**: 977–986.

Ericka, M., Vasic, D., Costa, F., Poulin, G. and Tliba, S. (2005). Energy Harvesting from Vibration Using a Piezoelectric Membrane, *J. Phys. IV France* **128**: 187–193.

Fang, H. B., Liu, J. Q., Xu, Z. Y., Dong, L., Chen, D., Cai, B. C. and Liu, Y. (2006). A MEMS-Based Piezoelectric Power Generator for Low Frequency Vibration Energy Harvesting, *Chinese Physics Letters* **23**: 732–734.

Feng, G. H. (2007). A Piezoelectric Dome-shaped-diaphragm Transducer for Microgenerator Applications, *Smart Materials and Structures* **16**: 2636–2644.

Goldfarb, M. and Jones, L. D. (1999). On the Efficiency of Electric Power Generation with Piezoelectric Ceramic, *Trans. ASME, Journal of Dynamic Systems, Measurement, and Control* **121**: 566–571.

Granstrom, J., Feenstra1, J., Sodano, H. A. and Farinholt, K. (2007). Energy Harvesting from a Backpack Instrumented with Piezoelectric Shoulder Straps, *Smart Materials and Structures* **16**: 1810–1820.

Guan, M. J. and Liao, W. H. (2007). On the Efficiencies of Piezoelectric Energy Harvesting Circuits towards Storage Device Voltages, *Smart Materials and Structures* **16**: 498–505.

Guigon, R., Chaillout, J. J., Jager, T. and Despesse, G. (2008a). Harvesting Raindrop Energy: Experimental Study, *Smart Materials and Structures* **17**: 015039.

Guigon, R., Chaillout, J. J., Jager, T. and Despesse, G. (2008b). Harvesting Raindrop Energy: Theory, *Smart Materials and Structures* **17**: 015038.

Guyomar, D., Badel, A., Lefeuvre, E. and Richard, C. (2005). Toward Energy Harvesting Using Active Materials and Conversion Improvement by Nonlinear Processing, *IEEE Transaction on Ultrasonics, Ferroelectrics, and Frequency Control* **52**: 584–595.

Hagood, N. W., Chung, W. H. and Flotow, A. V. (1990). Modelling of Piezoelectric Actuator Dynamics for Active Structural Control, *Journal of Intelligent Material Systems and Structures* **1**: 327–354.

Horowitz, S. B., Sheplak, M., III, L. N. C. and Nishida, T. (2006). A MEMS Acoustic Energy Harvester, *Journal of Micromechanics and Microengineering* **16**: S174–S181.

Hu, H. P., Cao, J. G. and Cui, Z. J. (2007). Performance of a Piezoelectric Bimorph Harvester with Variable Width, *Journal of Mechanics* **23**: 197–202.

Hu, H. P., Xue, H. and Hu, Y. T. (2007a). A Spiral-Shaped Harvester with an Improved Harvesting Element and an Adaptive Storage Circuit, *IEEE Transaction on Ultrasonics, Ferroelectrics, and Frequency Control* **54**: 1177–1187.

Hu, Y. T., Xue, H. and Hu, H. P. (2007b). A Piezoelectric Power Harvester with Adjustable Frequency through Axial Preloads, *Smart Materials and Structures* **16**: 1961–1966.

Jeon, Y. B., Sood, R., Jeong, J. H. and Kim, S. G. (2005). MEMS Power Generator with Transverse Mode Thin Film PZT, *Sensors and Actuators* A **122**: 16–22.

Jiang, S., Li, X., Guo, S., Hu, Y., Yang, J. and Jiang, Q. (2005). Performance of a Piezoelectric Bimorph for Scavenging Vibration Energy, *Smart Materials and Structures* **14**: 769–774.

Johnson, T. J. and Clark, W. W. (2005). Harvesting Energy from Piezoelectric Material, *IEEE Pervasive Computing* **4**: 70–71.

Kansal, A. and Srivastava, M. B. (2005). Distributed Energy Harvesting for Energy-Neutral Sensor Networks, *IEEE Pervasive Computing* **4**: 69–70.

Kim, H. W., Batra, A., Priya, S., Uchino, K., Markley, D., Newnham, R. E. and Hofmann, H. F. (2004). Energy Harvesting Using a Piezoelectric "Cymbal" Transducer in Dynamic Environment, *Japanese Journal of Applied Physics* **43**: 6178–6183.

Kim, H. W., Priya, S., Uchino, K. and Newnham, R. E. (2005). Piezoelectric Energy Harvesting under High Pre-Stressed Cyclic Vibrations, *Journal of Electroceramics* **15**: 27–34.

Kim, S., Clark, W. W. and Wang, Q. M. (2005a). Piezoelectric Energy Harvesting with a Clamped Circular Plate: Analysis, *Journal of Intelligent Material Systems and Structures* **16**: 847–854.

Kim, S., Clark, W. W. and Wang, Q. M. (2005b). Piezoelectric Energy Harvesting with a Clamped Circular Plate: Experimental Study, *Journal of Intelligent Material Systems and Structures* **16**: 855–863.

Kuo, A. D. (2005). Harvesting Energy by Improving the Economy of Human Walking, *Science* **309**: 1686–1687.

Lee, C. K., Hsu, Y. H., Hsiao, W. H. and Wu, J. W. J. (2004). Electrical and Mechanical Field Interactions of Piezoelectric Systems: foundation of smart structures-based piezoelectric sensors and actuators, and free-fall sensors, *Smart Materials and Structures* **13**: 1090–1109.

Lefeuvre, E., Badel, A., Benayad, A., Lebrun, L., Richard, C. and Guyomar, D. (2005a). A Comparison between Several Approaches of Piezoelectric Energy Harvesting, *Journal de Physique IV. France* **128**: 177–186.

Lefeuvre, E., Badel, A., Richard, C. and Guyomar, D. (2005b). Piezoelectric Energy Harvesting Device Optimization by Synchronous Electric Charge Extraction, *Journal of Intelligent Material Systems and Structures* **16**: 865–876.

Lefeuvre, E., Badel, A., Richard, C., Petit, L. and Guyomar, D. (2006). A Comparison between Several Vibration-Powered Piezoelectric Generators for Standalone Systems, *Sensors and Actuators A* **126**: 405–416.

Leland, E. S. and Wright, P. K. (2006). Resonance Tuning of Piezoelectric Vibration Energy Scavenging Generators Using Compressive Axial Preload, *Smart Materials and Structures* **15**: 1413–1420.

Lesieutre, G. A. and Davis, C. L. (1997). Can a Coupling Coefficient of a Piezoelectric Device be Higher than Those of its Active Material?, *Journal of Intelligent Material Systems and Structures* **8**: 859–867.

Lesieutre, G. A., Ottman, G. K. and Hofmann, H. F. (2004). Damping as a Result of Piezoelectric Energy Harvesting, *Journal of Sound and Vibration* **269**: 991–1001.

Liao, W. H., Wang, D. H. and Huang, S. L. (2001). Wireless Monitoring of Cable Tension of Cable-Stayed Bridges Using PVDF Piezoelectric Films, *Journal of Intelligent Material Systems and Structures* **12**: 331–339.

Liu, W. Q., Feng, Z. H., He, J. and Liu, R. B. (2007). Maximum Mechanical Energy Harvesting Strategy for a Piezoelement, *Smart Materials and Structures* **16**: 2130–2136.

Lu, F., Lee, H. P. and Lim, S. P. (2004). Modeling and Analysis of Micro Piezoelectric Power Generators for Micro-Electro-Mechanical-Systems Applications, *Smart Materials and Structures* **13**: 57–63.

Makihara, K., Onoda, J. and Miyakawa, T. (2006). Low Energy Dissipation Electric Circuit for Energy Harvesting, *Smart Materials and Structures* **15**: 1493–1498.

Mateu, L. and Moll, F. (2005). Optimum Piezoelectric Bending Beam Structures for Energy Harvesting Using Shoe Inserts, *Journal of Intelligent Material Systems and Structures* **16**: 835–845.

Mossi, K., Green, C., Ounaies, Z. and Hughes, E. (2005). Harvesting Energy Using a Thin Unimorph Prestressed Bender: Geometrical Effects, *Journal of Intelligent Material Systems and Structures* **16**: 249–261.

Muriuki, M. G. and Clark, W. W. (2007). Analysis of a Technique for Tuning a Cantiliver Beam Resonator Using Shunt Switching, *Smart Materials and Structures* **16**: 1527–1533.

Nakano, K., Elliott, S. J. and Rustighi, E. (2007). A Unified Approach to Optimal Conditions of Power Harvesting using Electromagnetic and Piezoelectric Transducers, *Smart Materials and Structures* **16**: 948–958.

Ng, T. H. and Liao, W. H. (2005). Sensitivity Analysis and Energy Harvesting for a Self-Powered Piezoelectric Sensor, *Journal of Intelligent Material Systems and Structures* **16**: 785–797.

Ngo, K. D., Phipps, A., Nishida, T., Lin, J. and Xu, S. (2006). Power Converters for Piezoelectric Energy Extraction, *Proceedings of 2006 ASME International Mechanical Engineering Congress and Exposition*, pp. IMECE2006–14343.

Ottman, G. K., Hofmann, H. F., Bhatt, A. C. and Lesieutre, G. A. (2002). Adaptive Piezoelectric Energy Harvesting Circuit for Wireless Remote Power Supply, *IEEE Transactions on Power Electronics* **17**: 669–676.

Ottman, G. K., Hofmann, H. F. and Lesieutre, G. A. (2003). Optimized Piezoelectric Energy Harvesting Circuit Using Step-Down Converter in Discontinuous Conduction Mode, *IEEE Transactions on Power Electronics* **18**: 696–703.

Poulin, G., Sarraute, E. and Costa, F. (2004). Generation of Electric Energy for Portable Devices: Comparative Study of an Electromagnetic and a Piezoelectric system, *Sensors and Actuators* A **116**: 461–471.

Prabhakar, S. and Vengallatore, S. (2007). Thermoelastic Damping in Bilayered Micromechanical Beam Resonators, *Journal of Micromechanics and Microengineering* **17**: 532–538.

Priya, S. (2005). Modeling of Electric Energy Harvesting Using Piezoelectric Windmill, *Applied Physics Letters* **87**: 184101.

Priya, S., Chen, C. T., Fye, D. and Zahnd, J. (2005). Piezoelectric Windmill: A Novel Solution to Remote Sensing, *Japanese Journal of Applied Physics* **44**: L104–L107.

Rabaey, J. M., Ammer, M. J., da Silva Jr., J. L., Patel, D. and Roundy, S. (2000). PicoRadio Supports Ad Hoc Ultra-Low Power Wireless Networking, *Computer* **33**: 42–48.

Ramsay, M. J. and Clark, W. W. (2001). Piezoelectric Energy Harvesting for Bio MEMS Applications, *Proceedings of the SPIE*, Vol. **4332**, pp. 429–438.

Renaud, M., Fiorini, P. and Hoof, C. V. (2007). Optimization of a Piezoelectric Unimorph for Shock and Impact Energy Harvesting, *Smart Materials and Structures* **16**: 1125–1135.

Richards, C. D., Anderson, M. J., Bahr, D. F. and Richards, R. F. (2004). Efficiency of Energy Conversion for Devices Containing a Piezoelectric Component, *Journal of Micromechanics and Microengineering* **14**: 717–721.

Richter, B., Twiefel, J., Hemsel, T. and Wallaschek, J. (2006). Model based Design of Piezoelectric Generators Utilizing Geometrical and Material Properties, *Proceedings of 2006 ASME International Mechanical Engineering Congress and Exposition*, pp. IMECE2006–14862.

Rome, L. C., Flynn, L., Goldman, E. M. and Yoo, T. D. (2005). Generating Electricity while Walking with Loads, *Science* **309**: 1725–1728.

Roundy, S. (2005). On the Effectiveness of Vibration-Based Energy Harvesting, *Journal of Intelligent Material Systems and Structures* **16**: 809–823.

Roundy, S., Leland, E. S., Baker, J., Carleton, E., Reilly, E., Lai, E., Otis, B., Rabaey, J. M., Wright, P. K. and Sundararajan, V. (2005). Improving Power Output for Vibration-Based Energy Scavengers, *IEEE Pervasive Computing* **4**: 28–36.

Roundy, S., Steingart, D., Frechette, L., Wright, P. and Rabaey, J. (2004a). Power Sources for Wireless Sensor Networks, *Lecture Notes in Computer Science* **2920**: 1–17.

Roundy, S. and Wright, P. K. (2004). A Piezoelectric Vibration Based Generator for Wireless Electronics, *Smart Materials and Structures* **13**: 1131–1142.

Roundy, S., Wright, P. K. and Rabaey, J. (2003). A Study of Low Level Vibrations as Power Source for Wireless Sensor Nodes, *Computer Communications* **26**: 1131–1144.

Roundy, S., Wright, P. K. and Rabaey, J. M. (2004b). *Energy Scavenging for Wireless Sensor Networks with Special Focus on Vibrations*, Kluwer Academic Publishers, Boston.

Sebald, G., Pruvost, S. and Guyomar, D. (2008). Energy Harvesting based on Ericsson Pyroelectric Cycles in a Relaxor Ferroelectric Ceramic, *Smart Materials and Structures* **15**: 015012.

Shahruz, S. M. (2006). Design of Mechanical Band-Pass Filters with Large Frequency Bands for Energy Scavenging, *Mechatronics* **16**: 523–531.

Shenck, N. S. and Paradiso, J. A. (2001). Energy Scavenging with Shoe-Mounted Piezoelectrics, *IEEE Micro* **21**: 30–42.

Shu, Y. C. and Lien, I. C. (2006a). Analysis of Power Output for Piezoelectric Energy Harvesting Systems, *Smart Materials and Structures* **15**: 1499–1512.

Shu, Y. C. and Lien, I. C. (2006b). Efficiency of Energy Conversion for a Piezoelectric Power Harvesting System, *Journal of Micromechanics and Microengineering* **16**: 2429–2438.

Shu, Y. C., Lien, I. C. and Wu, W. J. (2007). An Improved Analysis of the SSHI Interface in Piezoelectric Energy Harvesting, *Smart Materials and Structures* **16**: 2253–2264.

Sodano, H. A., Inman, D. J. and Park, G. (2004). A Review of Power Harvesting from Vibration Using Piezoelectric Materials, *The Shock and Vibration Digest* **36**: 197–205.

Sodano, H. A., Inman, D. J. and Park, G. (2005a). Comparison of Piezoelectric Energy Harvesting Devices for Recharging Batteries, *Journal of Intelligent Material Systems and Structures* **16**: 799–807.

Sodano, H. A., Inman, D. J. and Park, G. (2005b). Generation and Storage of Electricity from Power Harvesting Devices, *Journal of Intelligent Material Systems and Structures* **16**: 67–75.

Sodano, H. A., Lloyd, J. and Inman, D. J. (2006). An Experimental Comparison between Several Active Composite Actuators for Power Generation, *Smart Materials and Structures* **15**: 1211–1216.

Sodano, H. A., Park, G. and Inman, D. J. (2004). Estimation of Electric Charge Output for Piezoelectric Energy Harvesting, *Journal of Strain* **40**: 49–58.

Starner, T. (1996). Human-Powered Wearable Computing, *IBM Systems Journal* **35**: 618–629.

Stephen, N. G. (2006a). On Energy Harvesting from Ambient Vibration, *Journal of Sound and Vibration* **293**: 409–425.

Stephen, N. G. (2006b). On Energy Harvesting from Ambient Vibration, *Proceedings of the Institution of Mechanical Engineers Part C - Journal of Mechanical Engineering Science* **220**: 1261–1267.

Taylor, G. W., Burns, J. R., Kammann, S. M., Powers, W. B. and Welsh, T. R. (2001). The Energy Harvesting Eel: A Small Subsurface Ocean/River Power Generator, *IEEE Journal of Oceanic Engineering* **26**: 539–547.

Trolier-Mckinstry, S. and Muralt, P. (2004). Thin Film Piezoelectrics for MEMS, *Journal of Electroceramics* **12**: 7–17.

Umeda, M., Nakamura, K. and Ueha, S. (1996). Analysis of the Transformation of Mechanical Impact Energy to Electric Energy Using Piezoelectric Vibrator, *Japanese Journal of Applied Physics* **35**: 3267–3273.

Umeda, M., Nakamura, K. and Ueha, S. (1997). Energy Storage Characteristics of a Piezo-Generator Using Impact Induced Vibration, *Japanese Journal of Applied Physics* **36**: 3146–3151.

Wang, Q. M. and Cross, L. E. (1999). Constitutive Equations of Symmetrical Triple Layer Piezoelectric Benders, *IEEE Transaction on Ultrasonics, Ferroelectrics, and Frequency Control* **46**: 1343–1351.

Wang, Q. M., Du, X. H., Xu, B. and Cross, L. E. (1999). Electromechanical Coupling and Output Efficiency of Piezoelectric Bending Actuators, *IEEE Transaction on Ultrasonics Ferroelectrics and Frequency Control* **46**: 638–646.

Wang, S., Lam, K. H., Sun, C. L., Kwok, K. W., Chan, H. L. W., Guo, M. S. and Zhao, X. Z. (2007). Energy Harvesting with Piezoelectric Drum Transducer, *Applied Physics Letters* **90**: 113506.

Whalen, S., Thompson, M., Bahr, D., Richards, C. and Richards, R. (2003). Design, Fabrication and Testing of the P^3 Micro Heat Engine, *Sensors and Actuators* A **104**: 290–298.

White, N. M., Glynne-Jones, P. and Beeby, S. P. (2001). A Novel Thick-Film Piezoelectric Micro-Generator, *Smart Materials and Structures* **10**: 850–852.

Williams, C. B. and Yates, R. B. (1996). Analysis of a Micro-Electric Generator for Microsystems, *Sensors and Actuators* A **52**: 8–11.

Xu, C. G., Fiez, T. S. and Mayaram, K. (2003). Nonlinear Finite Element Analysis of a Thin Piezoelectric Laminate for Micro Power Generation, *Journal of Microelectromechanical Systems* **12**: 649–655.

Yang, J., Chen, Z. and Hu, Y. T. (2007). An Exact Analysis of a Rectangular Plate Piezoelectric Generator, *IEEE Transaction on Ultrasonics Ferroelectrics and Frequency Control* **54**: 190–195.

Yeatman, E. M. (2007). Applications of MEMS in Power Sources and Circuits, *Journal of Micromechanics and Microengineering* **17**: S184–S188.

Yoon, H. S., Washington, G. and Danak, A. (2005). Modeling, Optimization, and Design of Efficient Initially Curved Piezoceramic Unimorphs for Energy Harvesting Applications, *Journal of Intelligent Material Systems and Structures* **16**: 877–888.

Zhao, X. and Lord, D. G. (2006). Application of the Villari Effect to Electric Power Harvesting, *Journal of Applied Physics* **99**: 08M703.